

Distribution Agreement

In presenting this thesis as a partial fulfillment of the requirements for a degree from Emory University, I hereby grant to Emory University and its agents the non-exclusive license to archive, make accessible, and display my thesis in whole or in part in all forms of media, now or hereafter now, including display on the World Wide Web. I understand that I may select some access restrictions as part of the online submission of this thesis. I retain all ownership rights to the copyright of the thesis. I also retain the right to use in future works (such as articles or books) all or part of this thesis.

Brady Wu

April 11, 2020

Memory Effects in the Friction of Hydrogel Particles

by

Brady Wu

Justin Clifford Burton
Adviser

Physics Department

Justin Clifford Burton
Adviser

Eric Weeks
Committee Member

Khalid Salaita
Committee Member

2020

Memory Effects in the Friction of Hydrogel Particles

By

Brady Wu

Justin Clifford Burton

Adviser

An abstract of
a thesis submitted to the Faculty of Emory College of Arts and Sciences
of Emory University in partial fulfillment
of the requirements of the degree of
Bachelor of Science with Honors

Physics Department

2020

Abstract

Memory Effects in the Friction of Hydrogel Particles

By Brady Wu

Hydrogels are cross-linked polymer networks that can absorb and retain a large fraction of water, often up to 90 percent by weight. They are widely used in many engineering applications as well as agriculture industries due to their ultralow friction, biocompatibility, and chemical transport capabilities. Previous research in our lab has identified and characterized three distinct regimes of friction in polyacrylamide (PAAm), polyacrylic acid (PAA), and agarose. Among other things, they have shown that around a critical velocity, the friction coefficient of hydrogels is reduced by an order of magnitude and displayed relaxation behavior over multiple timescales. Now, following upon that, we looked closer at the time dependent behavior of PAA gel. We have shown that this friction regime exhibits a nearly exponential decay sensitive to the sliding velocity and precedent shearing. In general, a higher sliding velocity will lead to a faster decay. We found multiple time scales in the friction decays. We have also found the recovery time of the PAA and agarose gels, which refers to the time it takes for the polymer network of the hydrogel to recover back to its initial unsheared state. Finally, we showed that the final state of the hydrogel is only determined by the external shear stress applied, no matter what the initial state of the hydrogel is. Our findings imply that we can tell from the current frictional behavior of hydrogel what kinds of shear the hydrogel has experienced. In other words, the hydrogel remembers, or has a "memory" of, the shear history it has been through.

Memory Effects in the Friction of Hydrogel Particles

By

Brady Wu

Justin Clifford Burton

Adviser

A thesis submitted to the Faculty of Emory College of Arts and Sciences
of Emory University in partial fulfillment
of the requirements of the degree of
Bachelor of Science with Honors

Physics Department

2020

Acknowledgements

I sincerely acknowledge Eric Weeks and Khalid Salaita for taking time out of their schedules to serve on my committee. Furthermore, I thankfully acknowledge all members of the Burton laboratory, especially Nicholas Cuccia, Suraj Pothineni, Joshua Mendez-Harper, and Guram Gogia, all of whom introduced and guided me to scientific research. I also want to acknowledge Effrosyni Seitaridou, who led me through my earliest path in Physics with her kindness and patience. Above all, I thank my advisor Justin Burton. As a first-year student with little knowledge in physics, Justin was willing to let me work in his lab and teach me all I know about research nowadays. He helped me find my future path to pursue a physics degree in graduate school. I cannot thank him enough for being such a kind and caring mentor.

Contents

1	Introduction	4
1.1	What is a Hydrogel?	4
1.2	Industrial Applications	4
1.3	Classical Friction	5
1.4	Friction of Hydrogel	6
1.4.1	Slow Velocity Regime	7
1.4.2	Time-dependent Regime	8
1.4.3	High Velocity Regime	9
1.5	Memory Effects in Friction	10
2	Methods	11
2.1	Tribometer Setup	11
2.2	Preparation of Hydrogels	14
2.2.1	Fabrication of Polyacrylamide Gels	14
2.2.2	Fabrication of Agarose Gels	14
2.2.3	Preparation of Polyacrylic acid Gels	15

3	Results and Discussion	16
3.1	Effective d of PAA Gel	16
3.2	Where is the Transition Regime?	18
3.3	Velocity Sensitive Decay	19
3.3.1	Experimental Protocol	19
3.3.2	Results	19
3.4	Recovery of Hydrogel	22
3.4.1	Experimental Protocol	22
3.4.2	Result	23
3.5	Shear Determines the State of PAA Gel	26
3.5.1	Experimental Protocol	26
3.5.2	Result	27
3.6	Proposed Model	28
4	Conclusion	31
5	Future Directions	32

List of Figures

1	Polymer network of Hydrogel	4
2	Friction Coefficient for Agarose and Polyacrylic acid Gels	7
3	Schematic diagram of hydrogel during experiment	8
4	Formation of bulk layer at high velocity	9
5	Tribometer in previous researches	11
6	Tribometer in this experiment	13
7	The effective pore size of PAA gel	17
8	The range of time dependent regime	18
9	Experimental protocol of multiple speed decay	20
10	Results of multiple speed decay	21
11	Experimental protocol of recovery of hydrogels	22
12	Recovery of PAA gel	23
13	Friction coefficient of PAA and agarose v.s. waiting time	25
14	Experimental protocol of relaxation from different initial conditions	26
15	Relaxation of hydrogels from different initial conditions	27
16	Schematic diagram of our proposed model	29

1 Introduction

1.1 What is a Hydrogel?

Hydrogels consist of a cross-linked hydrophilic polymer network saturated with fluid. The fluid keeps the polymer network from collapsing, and the polymer network prevents the fluid from flowing away. It is a material that has both solid and liquid characteristics. While it does have a definite shape and deform elastically, like a solid, there is internal solute diffusion and fluid dynamics, like a liquid. At the molecular scale, the polymer is entangled and crosslinked into a huge polymer network as shown in Figure 1. When it is dehydrated, all the polymers are collapsed together. Once it is immersed in a fluid, the polymer network expands as it absorbs and retains individual fluid molecules due to hydrogen bonding. Different solvent (water, alcohol, etc.) can be used for different gels, depending on the specific chemical structures of the polymer. If not immersed in fluid, fluid will evaporate, and the hydrogel will usually dry up completely within 15 hours [3].

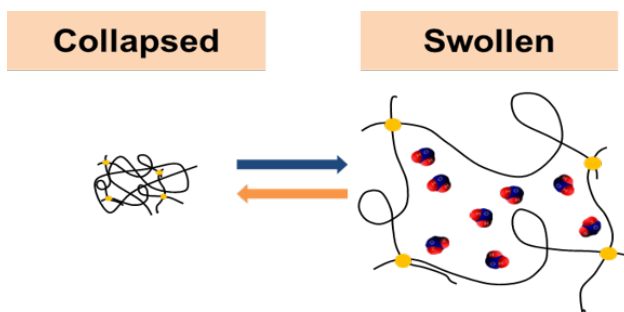


Figure 1: The polymer network of the hydrogel when it is dehydrated (left) and saturated with water(right). The yellow dots indicate the crosslinking sites. The polymer network expands as the hydrogel is hydrated. This process is reversible.

1.2 Industrial Applications

As the size of the fluid molecule (usually water) is on the order of angstroms, which is much smaller than the average pore size of the polymer network (around 100 nm), the individual

fluid molecule is free to move around in the polymer network, so is any solute dissolved in the fluid. This unique attribute is utilized in biology for a size-selective, diffusion-based DNA separation. As hydrogels also retain and preserve the fluid, they have been widely used in agricultural practices to replace or enhance conventional soil [10].

Furthermore, due to its ultralow friction, bio-compatibility, and soft nature, hydrogel is widely used in medical procedures and cartilage replacement [9, 27, 16, 13, 1], biomaterials [19, 21, 20, 26, 15, 5, 11, 14], and soft robotics [2, 30, 34]. Many of these applications depend sensitively on the tribological properties of the hydrogel, where interfacial rheology, polymer interaction with solvent and solid substrate constitute a rich spectrum of friction behavior [6].

1.3 Classical Friction

The investigation of friction between two dry solids can be traced back to ancient Greece, but it is not until 1700s, that people's understanding of classical friction solidifies. In general, there are three characteristics of friction between dry solids.

- The force of friction is directly proportional to the applied load.
- The force of friction is independent of the apparent area of contact.
- Kinetic friction is independent of the sliding velocity.

We are mostly concerned with the kinetic friction, which can be summarized as the equation below.

$$F_f = \mu F_n, \tag{1}$$

where F_f is the friction force, μ is the friction coefficient, and F_n is the normal force acting on the object. This equation shows that the magnitude of the friction really only depends on the normal force applied on the object and the surface properties of the two objects.

1.4 Friction of Hydrogel

The friction coefficient, μ , of a hydrogel is typically very low, often below 0.01 in laboratory-scale sliding velocities. Such low friction partially stems from the high volume fraction of solvent in the hydrogel, which allows for a subnanometer fluid layer to form, and potentially involves molecular slip at the interface [17, 24]. While the pore size distribution of the hydrogel can be polydisperse and depends on the exact chemical structure of the hydrogel, the average pore size of the hydrogel is of order 5-500 nm [29]. This is much larger than the average thickness of a fluid hydration layer (< 1 nm). Therefore, the fluid flow through the porous network of the hydrogel plays a significant role in the frictional properties of hydrogel and is often coupled to polymers dynamics and elasticity of the gel.

Three dominant factors are known to affect the friction of hydrogel. First, the hydrodynamics and elastic deformation of the hydrogels will matter. At slow velocity, Darcy-like flow through the porous hydrogel network is expected to exist at the interface. The elastic deformation of the hydrogel will also matter depending on contact geometry [28, 23, 35, 32, 31]. For example, the contact geometry between a soft ball and a hard solid substrate is flat, and that between a hard ball and soft solid substrate is curved. The elastic deformation of the latter case will affect the friction measured much more than the former case. Second, the physical and chemical properties of the hydrogels and the substrate also have an effect in friction. Depending on the strength of the interaction between polymers and solid substrate relative to that between polymers and the solvents, the polymers of the hydrogel will either be repelled from or adsorbed to the solid surface. It has been shown that when the interaction is more repulsive, the viscous flow of solvent in the porous hydrogel network will matter more,

whereas the deformation and adsorption of polymer chains on the solid substrate will have a bigger effect for adsorption [8]. Finally, the mechanical and thermodynamic properties of the polymer network, ie. surface roughness and polymer cross linking density, can affect the relaxation and hydration timescales [25, 22].

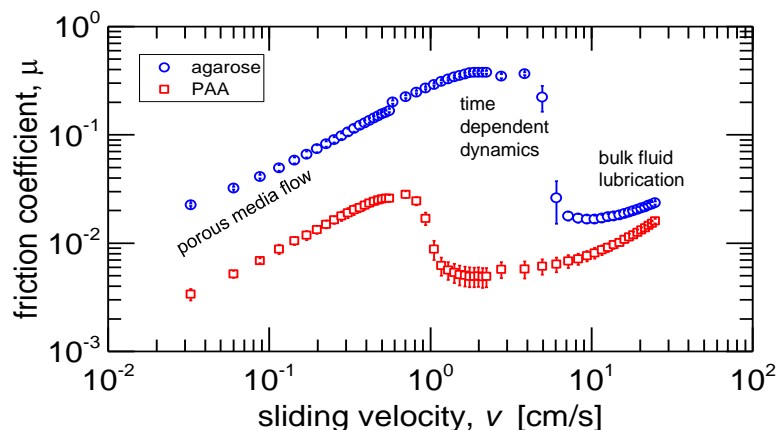


Figure 2: The friction coefficient of agarose and PAA gels on acrylic disk. Three different friction regimes can be seen in both agarose and PAA gels. The friction coefficient of agarose is generally higher than that of PAA. At slow velocity, the friction increases monotonically until it reaches a critical velocity, v_c , where the friction coefficient plummets by an order of magnitude. At high velocity, the friction is less dependent on the specific chemical properties of the hydrogels.

Three distinct regimes of friction have been identified in both agarose and PAA gels by Cuccia et al. [4], as shown in Figure 2. These three regimes have different friction mechanisms and display distinct mechanical behaviors that will be further explained below.

1.4.1 Slow Velocity Regime

At slow sliding velocity, the main source of friction is the fluid flow through the porous network of the hydrogel. As fluid is dragged through the polymer matrix, the fluid velocity decays over distance; we can approximate this decay as linear, such that the fluid velocity is v at the interface and linearly decays and vanishes over distance d , as shown in Figure 3, Newton's law of viscosity states that,

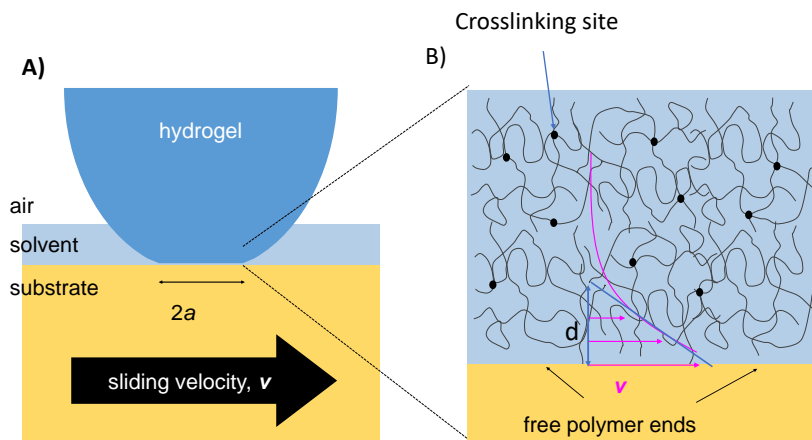


Figure 3: Schematic diagram of A) a hydrogel pressed against the substrate; the diameter of the contact area is $2a$. The substrate is moving relative to the hydrogel with a velocity v . B) the zoom in figure of hydrogel. As the substrate is sliding past the hydrogel, the velocity decays over distance. We can model this decay as linear, and d will be the characteristic distance over which the velocity decays.

$$F = \eta A \frac{v}{d}, \quad (2)$$

where η is the viscosity of the fluid, A is the contact area between the hydrogel and the solid surface, and d is the characteristic distance. Cuccia et al. have shown that this characteristic distance d is effectively the pore size of the hydrogel and that this approximation fits the experimental result as the friction coefficient of the hydrogel at low sliding velocity follows a power law of $F \propto v^\gamma$, where $0.5 < \gamma < 1.0$ [4].

1.4.2 Time-dependent Regime

As the sliding velocity further increases, the friction coefficient of the hydrogel does not increase monotonically as the equation 2 predicts. Instead, the friction coefficient peaks at a critical velocity, v_c , and plummets by often an order of magnitude over a relatively short span of sliding velocity, usually within a factor of 2. This friction regime displays strong time-dependent behavior with exponential decay that suggests one relaxation timescale, but depending on the experimental protocol, it is possible to observe relaxation over multiple

timescales; this will be discussed in the subsequent sections. We have found that both the peak friction coefficient and critical velocity depend on the running time, t_p , over which we average the raw data to obtain the friction force. However, a threshold sliding velocity does exist and there is a minimal shear needed to trigger this time-dependent behavior. Dunn et al. attributed this time-dependent behavior and friction transition to two potential reasons [12]: First, the shear applied on the hydrogel might lead to a alignment of surface polymer chains, reducing the friction. Second, dehydration of hydrogel due to pressure [25] could be recovered through a mechanism called "tribological rehydration" [22], lowering the friction. Cuccia et al. [4] have shown that rehydration is unlikely because the relaxation time scales for 50% sugar water and DI water are roughly the same, although 50% sugar water is 15 times more viscous than DI water.

1.4.3 High Velocity Regime

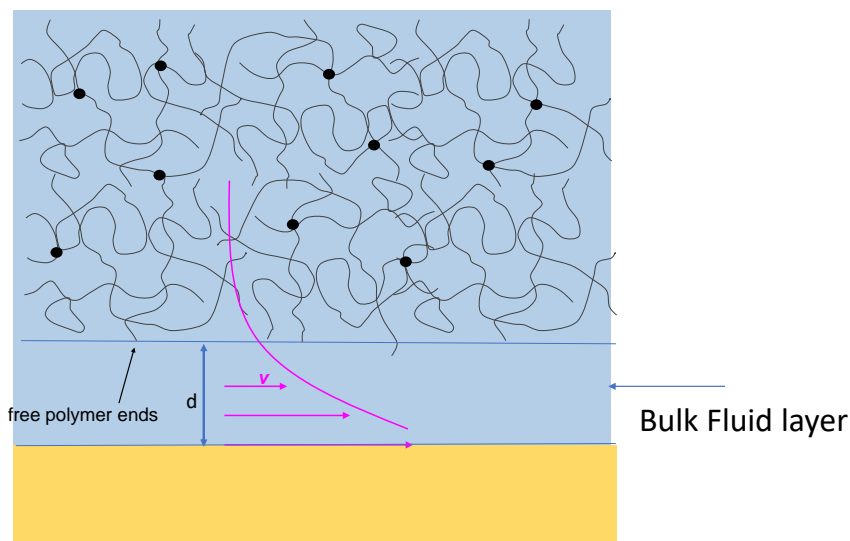


Figure 4: At high velocity, a bulk fluid layer builds up at the interface of hydrogel and the substrate. The thickness of the bulk layer is usually on the order of a few micrometer.

At higher sliding velocity, a bulk fluid layer, as shown in Figure 4, with a thickness on the order of micrometer begins to form due to the asymmetric deformation of the hydrogel

[33, 28, 31, 23]. This fluid layer is two orders of magnitude higher than the average pore size of the hydrogel. We can again apply equation 2 to approximate the magnitude of the shear force. However, the characteristic distance, d , here is approximately the thickness of the bulk fluid layer. Therefore, at high sliding velocity, the friction coefficient of the hydrogel is not related to the internal properties of the hydrogel, but to the viscosity of the fluid. These three regimes have been observed in polyacrylamide (PAAm), polyacrylic acid (PAA), and agarose, despite their different physical and chemical properties.

1.5 Memory Effects in Friction

My main objective in this research project was to explore the different competing effects in the transitional regime. We have found that beyond a threshold shear stress, the friction of the hydrogel decays exponentially. In general, a higher sliding velocity will lead to faster decay. We found multiple time scales in the friction decays. We have also found the relaxation time of the PAA and agarose gels, which refers to the time it takes for the polymer network of the hydrogel to recover back to its initial unsheared state. Finally, we showed that the eventual state of the hydrogel is only controlled by the external shear stress applied, no matter what the initial state of the hydrogel is. Our current model of entangled polymers at the hydrogel surface can well capture all of our observations, although it needs future experimental verifications.

2 Methods

2.1 Tribometer Setup

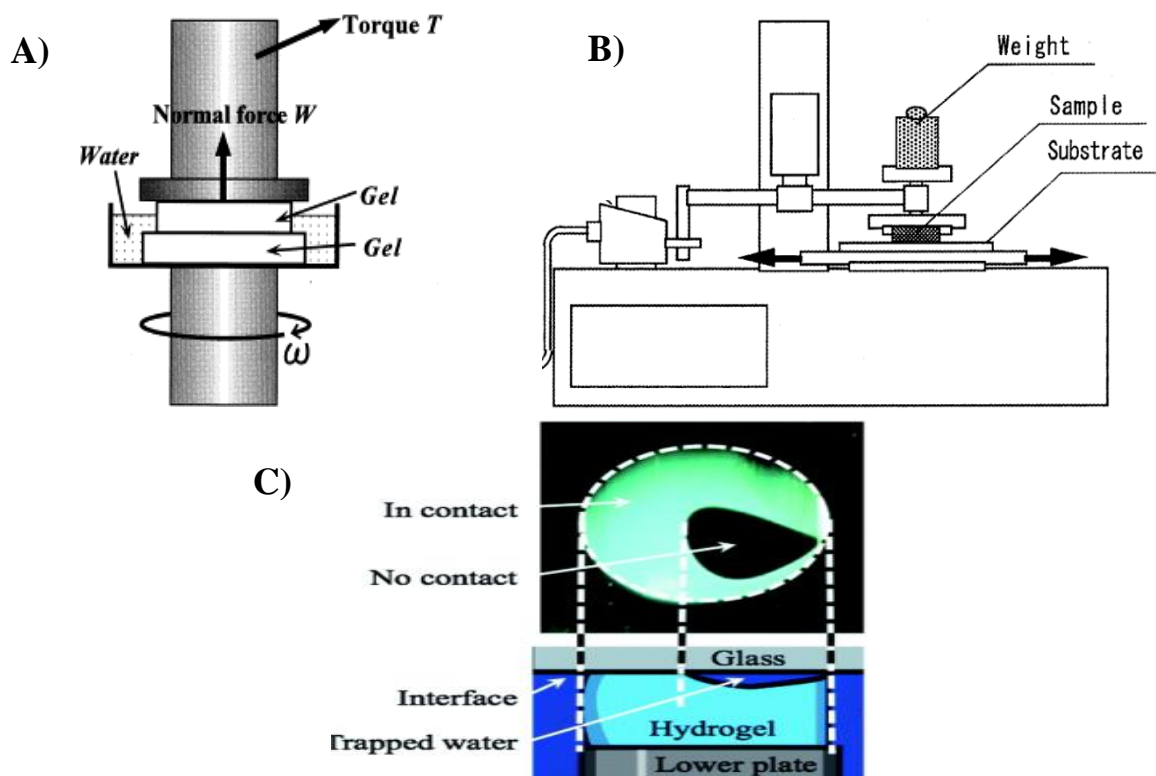


Figure 5: A) A tribometer that measures the friction by spinning two gel disks against each other [36]. B) A tribometer that measures the friction by pulling two slabs of gels against each other [7]. C) A figure showing the contact surface between hydrogel and glass; the contact surface is not homogeneous, as can be seen from the figure.

In the previous frictional studies of hydrogel, there are two kinds of tribological methods. Figure 5 A shows a setup that rotates two disks of hydrogels to obtain the friction; B shows one that pulls one slab of hydrogel against another. In both cases, there is not a homogeneous contact region. As shown in part C, water can be easily trapped between the disks or slabs of hydrogels, forming a bubble of water, which makes calculating the exact contact area very difficult [7]. Thus, an alternative tribological method that clearly defines the contact area should be developed.

Our experiment was performed on a custom pin-on-disk, bi-directional tribometer as illustrated in Figure 6 A [4]. This setup allows a well-defined circular contact area to form, as shown in Figure 3 A. The tribometer consists of an aluminum disk and on which the solid substrate is mounted. The disk was driven by a motor system and can rotate in both directions at a specified angular velocity ω . A spherical sample of hydrogel with radius $R \approx 7.5\text{mm}$ was held stationary to the end of a low-force strain sensor (Strain Measurement Devices S256). This strain sensor measured the tangential force (F_f) on the hydrogel and was calibrated before use. The cantilevered spherical hydrogel rested on the horizontal solid substrate. For all of our experiments, a cast acrylic was the solid substrate. A normal force, $F_n = 200\text{mN}$, was applied above the point of contact of the hydrogel using a fixed amount of mass under the influence of gravity. The friction coefficient is calculated as $\mu = \frac{F_f}{F_n}$. A macroscopic layer of solvent over the substrate, usually water unless specified otherwise, kept the hydrogel sample hydrated throughout the friction measurement. Part of the supporting aluminum plate below the solid substrate was removed to get an optical image of the contact between the hydrogel sample and the solid substrate, which allows for the measurement of the contact area [4].

Figure 6 B shows the motor system of the tribometer. A stepper motor that can rotate between 0.005 revolutions per second (rps) to 6 revolutions per second is used to drive the substrate. As one revolution of the stepper motor is typically divided into 200 steps, each one rotates the shaft by 1.8° . To reduce the level of noise caused by the discreteness of the steps at a low angular velocity, we use micro-steps, which is $\frac{1}{16}$ of the typical step size. In addition, since the highest rotation speed we use in the experiment is roughly 1 rps, we built a gear system to reduce the speed of the stepper motor by a factor by 5. This also further lowers our noise from the discreteness of the rotation. With the gear system, the linear sliding velocity we can obtain is 0.04 cm/s to 50 cm/s.

Data acquisition and motor control were accomplished via a custom LabVIEW program. For

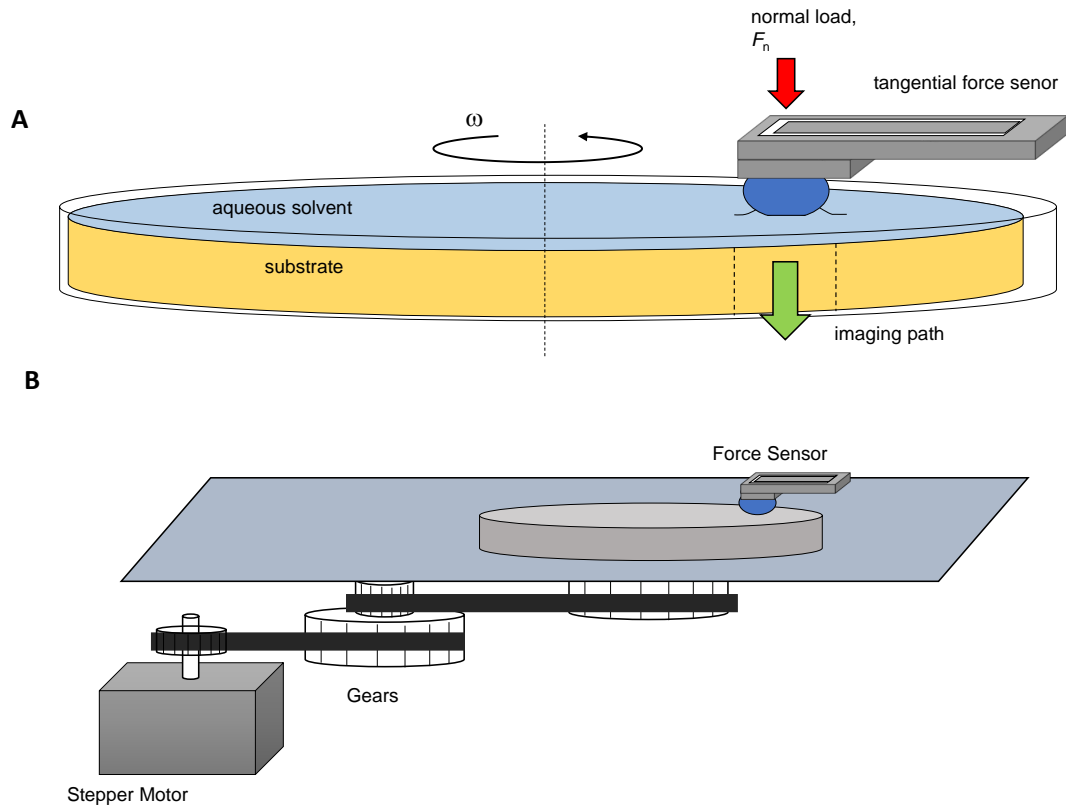


Figure 6: The basic setup of the experiment. A) the custom tribometer consists of an aluminum disk on which a solid substrate is mounted. The disk can rotate in both directions with a specified angular velocity ω . The hydrogel with a radius $R \approx 7.5\text{mm}$ is fixed to the end of the force sensor. Below the hydrogel, there is an imaging path that allows for a direct visual observation on the hydrogel. B) The motor system of the tribometer consists of a gear system, a stepper motor and the aluminum disk. The gear system reduces the speed of the stepper motor by a factor of 5.

each data point at a given sliding velocity, we ran the motor clockwise for $30\text{s} \leq t_p \leq 3600\text{s}$, paused for 5 seconds, and then ran the motor counterclockwise for the same t_p . Throughout the experiment, a USB data acquisition device (NI USB-6009) sampled the voltage reading from the strain sensor at 24 kHz for 0.5 s, and the resulting 12,000 data points were averaged to reduce noise. Thus, the friction coefficient data were sampled every 0.5 s. After one complete measurement of friction in both directions, we then switched to the next velocity. Measuring the friction in both directions allows us to calibrate the zero point of the friction measurement and check for any asymmetries in the friction measurement.

The final friction value for each sliding velocity is obtained by taking the average for all the data points during the measurement t_p in the clockwise direction f_{cl} and counterclockwise

direction f_{cou} . The final friction value, f , is therefore defined as

$$f = \frac{|f_{cl} + f_{cou}|}{2}.$$

All data were taken at $22 \pm 2^\circ C$.

2.2 Preparation of Hydrogels

We used three types of hydrogels for our experiments: polyacrylamide (PAAm), agarose, and commercial polyacrylic acid. We fabricated polyacrylamide and agarose gel in the lab and purchased the commercial polyacrylic acid gel from JRM Chemical (Cleveland, OH). All chemicals and solvents used for fabrication were purchased from Millipore Sigma.

2.2.1 Fabrication of Polyacrylamide Gels

We first dissolved the acrylamide/bis-acrylamide mixture (8-24% by weight) in 10ml of DI water. The solution was degassed for half an hour before an ammonium persulfate initiator (0.15% by weight) is added. We then added the tetramethylethylenediamine (TEMED) catalyst (0.15% by weight). The resulting solution was then pipetted into custom spherical silicone molds for gelation at room temperature over 10 hours. Once fully gelated, the hydrogel was immersed in DI water for 2 hours before each measurement.

2.2.2 Fabrication of Agarose Gels

We dissolved agarose solid (0.5-2% by weight) in 100ml of DI water. After the solution was well mixed, we heated it to boiling temperature for 1 minute in a lab microwave. The resulting solution was cooled down at room temperature for 20 minutes. The solution was

then pipetted into custom spherical silicone molds for gelation at room temperature over 2 hours. The hydrogel was immersed in DI water for 2 hours before each measurement.

2.2.3 Preparation of Polyacrylic acid Gels

The PAA gels are purchased from JRM Chemical (Cleveland, OH). The gel beads are immersed in DI water for at least 16 hours before measurements. The polymer content of PAA gel when fully swelled is 0.8% by weight, which means that 99.2% of the gel is made of water.

3 Results and Discussion

3.1 Effective d of PAA Gel

Here we offer another way to look at the friction of hydrogel. From equation 2, we can calculate the effective pore size d . The friction force is measured during the experiment, sliding velocity is the control parameter, and we can calculate the contact area of PAA gel using Hertzian contact theory. Hertzian contact theory predicts that when a soft ball is pressed against a hard solid surface, the radius a as shown earlier in Figure 3 A, of contact area between these two objects will be

$$a^3 = \frac{3F_n R}{4E^*}, \quad (3)$$

where F_n is the normal force on the object, R is the radius of the PAA gel and E^* is the reduced average modulus for the PAA gel and solid substrate:

$$\frac{1}{E^*} = \frac{1 - \nu_g^2}{E_g} + \frac{1 - \nu_s^2}{E_s}. \quad (4)$$

Here E and ν are the Young's modulus and Poisson's ratio for the gel (g) and substrate (s).

The contact area for a normal PAA gel with radius 7.5 mm, elastic modulus 45 kPa [4], and normal force 0.2 N is $2.69 \times 10^{-5} m^2$ or $26.9 mm^2$.

Thus, using the contact area, friction force for every velocity, and $\eta = 1 mPa.s$, we can calculate the effective pore size d for all of the sliding velocities. The result is shown in Figure 7.

Figure 7 B shows the value of d calculated for all sliding velocity. At slow velocity, d stays roughly constant, and this value is defined as the actual pore size of the hydrogel in our

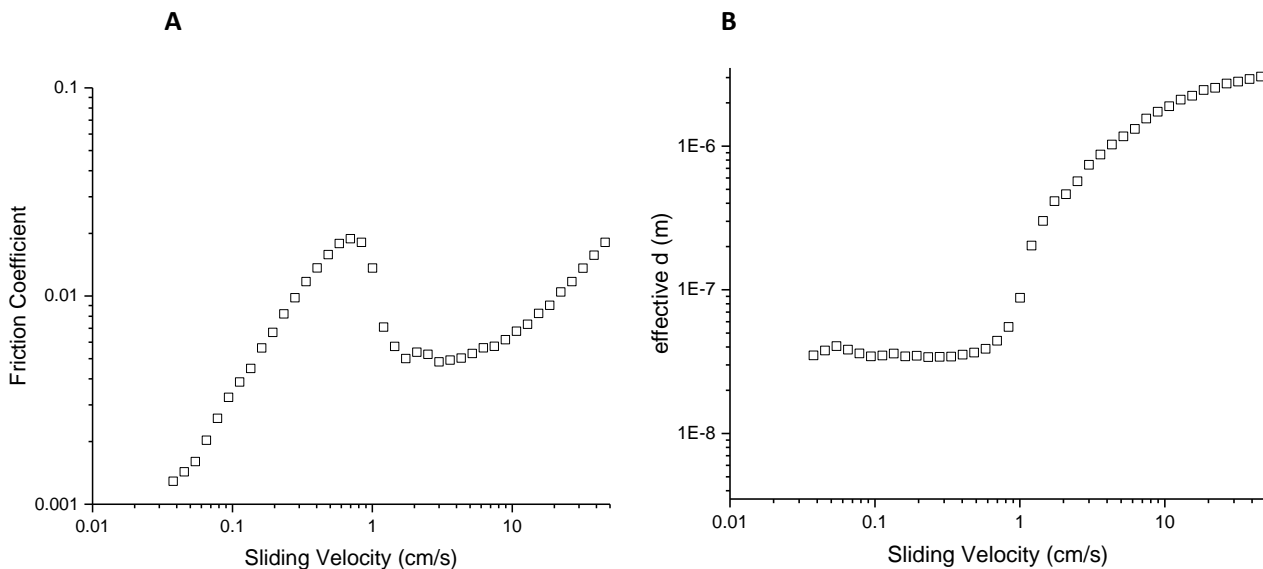


Figure 7: A) a conventional friction coefficient measurement for PAA gel on acrylic surfaces with $t_p = 30s$. B) The effective pore size d calculated using the data from A). For slow velocity, the effective pore size is roughly constant, it starts to escalate at $v \approx 1cm/s$, which is around the critical velocity for A). As velocity further increases, the value of d is approaching a constant value again.

experiment. This constant pore size is equivalent to the constant slope of 1 in Figure 7 A. At the critical velocity, the magnitude of friction coefficient plummets by an order of magnitude; thus, the effective pore size of the hydrogel increases by an order of magnitude. The actual pore size of the hydrogel might not change that much, but there is a structural change happening at the surface of hydrogel that effectively increases the length scale d . As the velocity increases further, the effective pore size d is approaching a constant value again. This value approached is the thickness of the bulk fluid film. From Figure 7 we can see that the pore size of PAA gel is roughly 40 nm while the thickness of the fluid film is on the order of 3 micrometers.

3.2 Where is the Transition Regime?

It could be hard to tell directly from Figure 2 where exactly time-dependent behavior takes place. We therefore vary the running time, t_p , or the time we spent at each velocity.

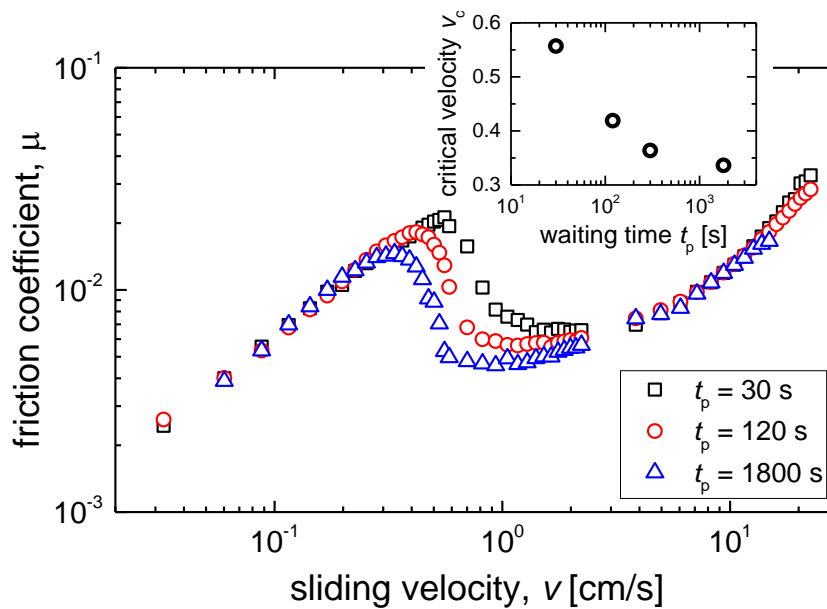


Figure 8: The friction coefficient of a PAA gel on an acrylic disk. We vary the running time, t_p , for the different sets of the experiments. Changing the t_p only affects the friction coefficient for $0.2 < v < 20$ cm/s. In this speed range, higher running time lowers the friction coefficient. The critical velocity, v_c , also decreases for higher t_p .

As can be seen from Figure 8, changing t_p only affects the friction coefficient for $0.2 < v < 20$ cm/s. Outside this range, the friction coefficient perfectly collapses onto each other, which means they are really time-independent. This makes sense because, at slow velocity, friction mainly comes from Darcy like flow; as the shear applied to the hydrogel is not enough to structurally change the hydrogel interface, the friction will be time-invariant. At high sliding velocity, the friction is dominant by the bulk fluid layer. As the thickness of this layer is only dependent on sliding velocity, the friction is also time-independent according to equation 2.

It also needs to be noted that the difference in μ is maximized at v_c for $t_p = 30s$; here, μ for $t_p = 30s$ has not yet started to drop, while the μ for $t_p = 1800s$ has reached the trough. Starting from the critical velocity for $t_p = 1800s$, the μ starts to diverge, and the difference

is maximized at v_c for $t_p = 30s$. As sliding velocity further increases, the friction coefficients start to converge again. This diverging and then converging behavior implies that there are relaxation processes in the friction decay whose timescales depend sensitively on the sliding velocity.

3.3 Velocity Sensitive Decay

3.3.1 Experimental Protocol

To explore how the friction decay behavior depends on sliding velocity, we continuously measure the friction coefficient of the hydrogel at an initial velocity v_i for 1800 s. The hydrogel is then allowed to relax for 2 hours and reset it to its unsheared state. We then measure the μ of the hydrogel at a new speed v , which is 1.5 times the previous speed. This process continues until the velocity reaches the maximum velocity v_m . This protocol is shown in the flow chart of Figure 9 A. Figure 9 B shows the the speed range in the context of the overall friction coefficient.

3.3.2 Results

After obtaining the μ , we then normalize the data for each set of the experiment for comparison by dividing the current μ by the maximum μ . Since the friction is decaying, the leftmost point will be the highest data point in every data set, and it will be 1 since we are dividing μ_{max} by μ_{max} .

As Figure 10 A shows, the friction decay does depend sensitively on sliding velocity. If we use equation

$$\mu = A + Be^{-\frac{t}{\tau}} \quad (5)$$

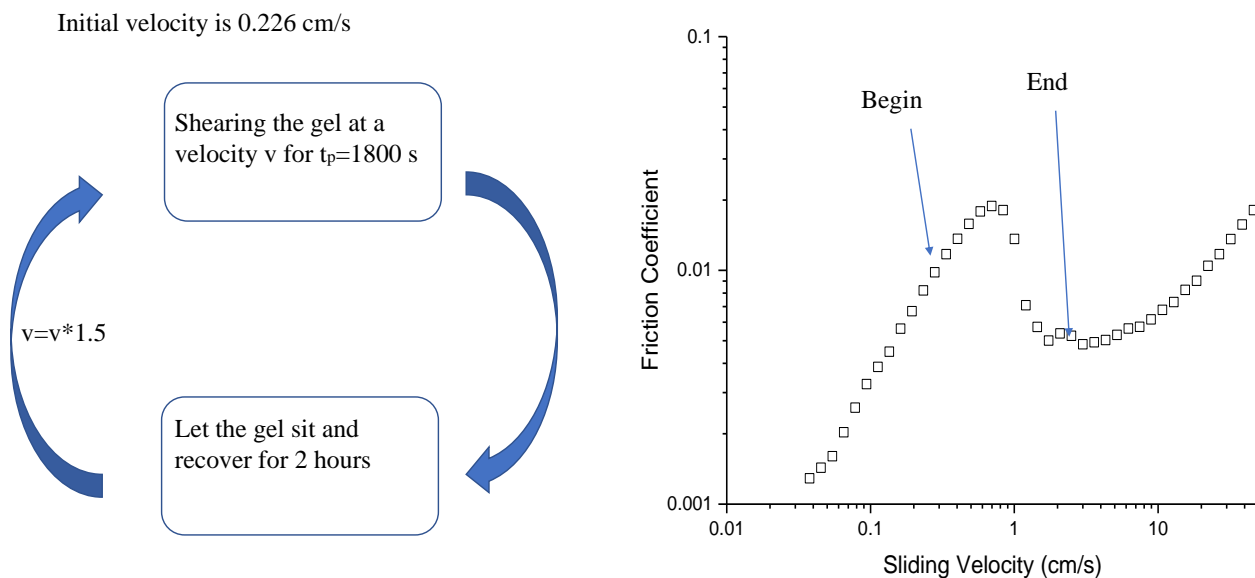


Figure 9: A) A flow chart of the experimental protocol. The initial sliding velocity used is 0.226 cm/s. Each new velocity is 1.5 times the previous velocity. B) A typical μ v.s. sliding velocity graph; it shows the beginning and end velocity and μ .

to perform curve fitting for each set of the experiment, we can obtain the decay time τ . The decay time τ is plotted against the sliding velocity in figure 10 C, and we can see that τ decreases as sliding velocity increases, meaning that the friction coefficient is decaying faster at higher sliding velocity. This observation agrees with what Figure 8 implies. We can see that the time constant is linear in the log y axis plot. This implies that the time constant is decaying exponentially. We can also see that in Figure 10 B, for $v = 1.27\text{cm/s}$ and $v = 1.9\text{cm/s}$, while the exponential fitted curve has reached its final constant value, the value of μ continues to decay more or less linearly. This implies that in the really long time scale, the friction coefficient exhibits logarithmic decay behavior, which is a characteristic of glassy materials.

It also needs to be noted that the extents of the decay also vary with sliding velocity, as shown in Figure 10 D. A is the fitting constant in equation 5; it represents the final value of $\frac{\mu}{\mu_{max}}$,

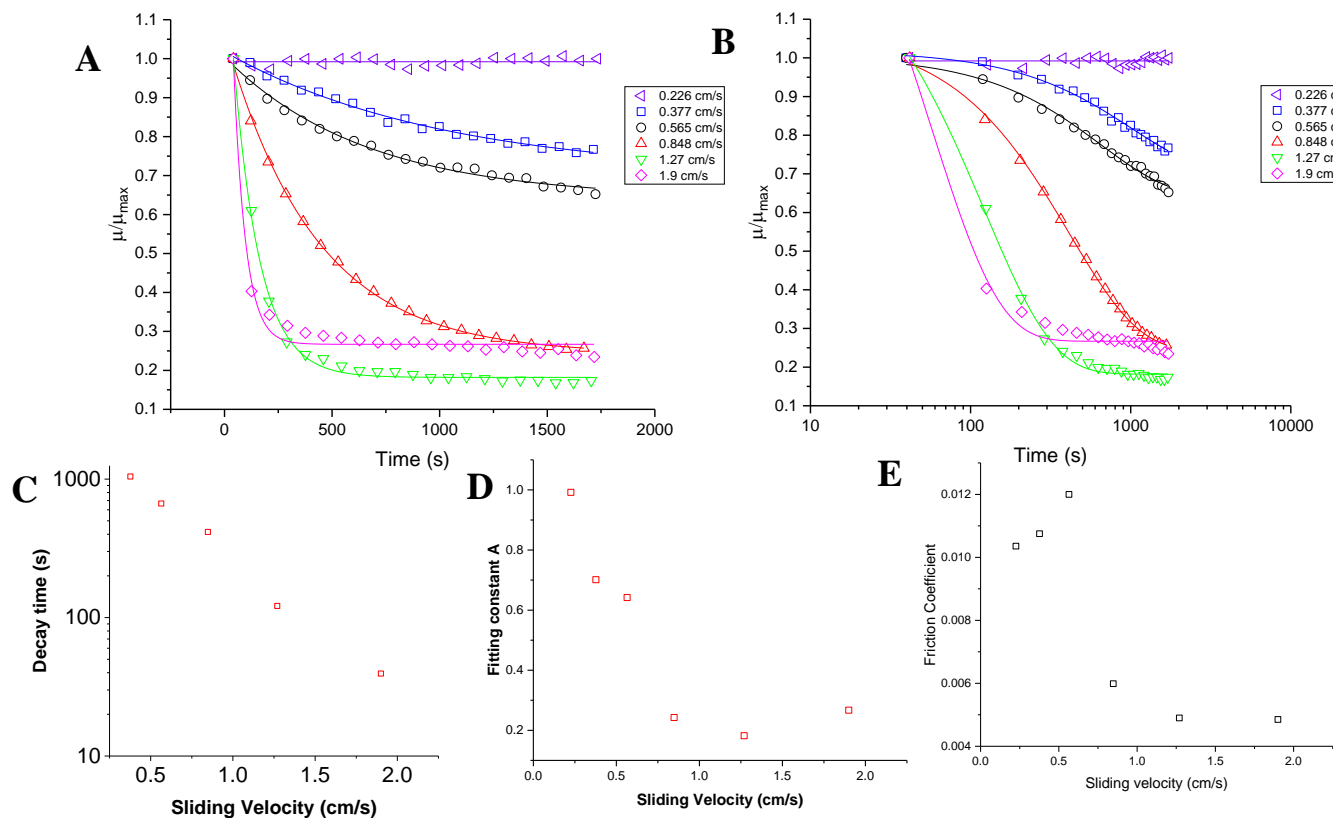


Figure 10: A) Normalized friction coefficient of PAA gel v.s. time. Every data point is normalized for comparison by dividing by the largest friction coefficient in the given set. All data are fitted with equation 5. B) The same data are plotted in a log time axis. C) the decay time τ v.s. sliding velocity in a log y-axis plot. Each set of the experiment is performed without any previous shearing. D) Fitting constant A v.s. sliding velocity. It can be seen that the fitting constant A decreases by a factor of 2 between 0.565 cm/s and 0.848 cm/s. E) The fitting constant $A^*\mu_{max}$ v.s. sliding velocity.

or the extent of shearing, as $t \rightarrow \infty$. When the sliding velocity is smaller than 0.565 cm/s, the friction coefficient only decays to around 60% of its maximum value. However, when the sliding velocity is further increased, μ is able to decay to around 20% of its maximum value. There is a huge change in the extent of the decay that happens within a narrow window of sliding velocity. This seems to suggest the hydrogel is undergoing some structural change above a threshold shear. Below this critical shear stress, the structural change is either happening very slowly and to a minimal extent or not happening at all. The actual friction coefficient in Figure 10 D is shown in E. The value of μ is obtained by multiplying A with μ_{max} . This will give us the value of μ as $t \rightarrow \infty$, assuming the μ follows an exponential decay trend. This plot mirrors the μ in Figure 8 for μ of $t_p = 1800s$. However, there is a

huge and abrupt change in μ at $v = 0.848\text{cm/s}$. The μ then reaches a constant as the μ for the two subsequent speeds are almost the same.

3.4 Recovery of Hydrogel

3.4.1 Experimental Protocol

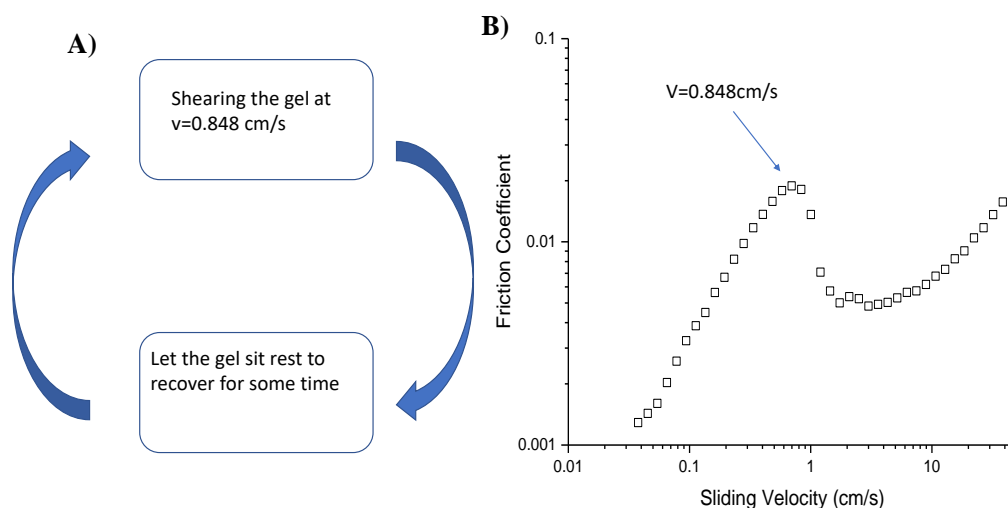


Figure 11: A) The experimental protocol. The time that hydrogel is allowed to relax is defined as the wait time. B) A typical friction coefficient graph v.s. sliding velocity. $v=0.848\text{ cm/s}$ is indicated in the graph.

While hydrogel will undergo a structural change when the shear stress is above the critical shear stress, we have also found that hydrogels will recover back to its unsheared state given sufficient time. Therefore, we looked at how the friction coefficient of PAA hydrogel behaves when it was given different amounts of time to relax after being sheared. Figure 11 A shows the experimental protocol. The time that hydrogel is given to recover is 60 s, 360s, and 1800s.

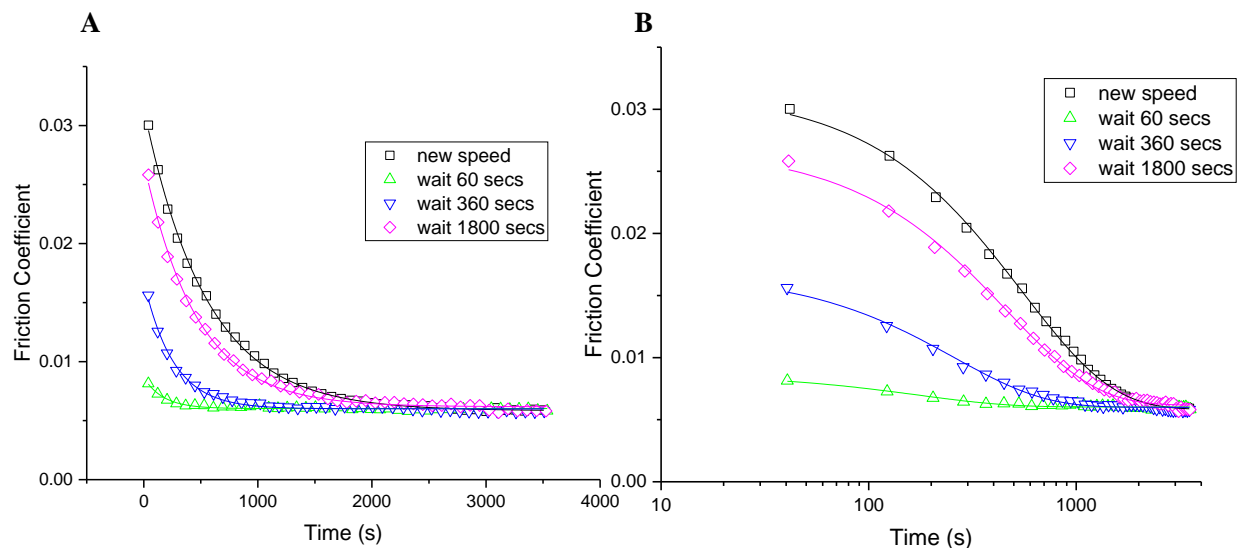


Figure 12: A) The friction coefficient of PAA gel v.s. time. B) Friction coefficient of PAA gel v.s. time on a log x-axis. New speed represents the friction coefficient of the hydrogel when it does not undergo any prior shearing. 60 s, 360 s, and 1800 s refer to the time that the hydrogel is allowed to relax after the previous run. The experiment is carried out in the order of new speed, wait 60 s, wait 360 s, and wait 1800 s. All data are fitted with equation 5.

3.4.2 Result

Figure 12 shows the friction coefficients of PAA hydrogel when it is given different amounts of time to relax after being completely sheared. New speed means that the hydrogel does not experience any shearing before the measurement; this is equivalent to the friction coefficient of hydrogel when it is given $t = \infty$ to relax. From the figure, we can see that the μ for all sets of experiments approach and collapse to the same value of μ after $t > 2000s$. However, once the hydrogel is given some time to relax, it rapidly recovers. Generally, if the gel is given longer time to recover, it will take longer time to decay. Thus, when the hydrogel does not have any prior shearing, or waiting time $\rightarrow \infty$, the μ takes the longest time to decay, or the largest τ according to equation 5. When the hydrogel is given a longer time to recover, the friction coefficient curves tend to approach the unsheared μ curve. The figure implies that the recovery rate tends to decrease since it recovers faster for smaller waiting times and

approaches 0 as $t_{wait} \rightarrow \infty$ when it reaches its unsheared state.

We can further explore how different amounts of wait time, the time to recover, will affect μ . Figure 12 shows that if the gel is given a longer time to recover, μ curve will have a longer decay and larger τ ; at the same time, if μ is recovering slower, it will spend a longer time at the higher μ values, and if we take the average for the whole range of t_p , the average μ will be higher. We can thus quantify the current state of the hydrogel with the average μ we measured and the decay constant τ . While the average value of μ will be dependent on the running time, t_p , spent at each sliding velocity, τ is independent of t_p . Both of these values will be shown in the results for PAA gels.

The experimental protocol for the results shown below is basically the same as the one shown in Figure 11. However, instead of having the actual running time on the x axis, we will have the wait time, the time the hydrogel is given to relax, on the x axis. This will directly show the recovery process as a function of wait time.

Here we measured the μ for $t_p = 600s$. If we fit the μ curve, we can get the constant τ and B as defined in equation 5, which are independent of the measurement time t_p . The resulting values for τ and B for each velocities are shown in Figure 13 A. Surprisingly, the constant B recovers faster than τ . If we apply the equation 5 again, we can get the time constant for B and τ , which are 460 secs and 1070 secs respectively. Although the average μ is dependent on the measurement time t_p , if we keep the t_p constant, we can get a rough idea of the recovery behaviors for PAA and agarose gels. It can be seen that μ and τ follows the same trend overall in Figure 13 B, although this is mainly coincidence. The recovery is exponential, as Figure 12 suggests. If we compare Figure 13 B and C, we can see that PAA gel takes much longer than agarose to fully recover. In fact, if we apply equation 5 to perform an exponential curve fitting for the μ of PAA gel and agarose gel, we can get decay constant 1850 secs for PAA gel and 630 secs for agarose gel. Thus, agarose gel is recovering three times as fast as PAA gel. We only measured the average μ for agarose since the decay mechanism for

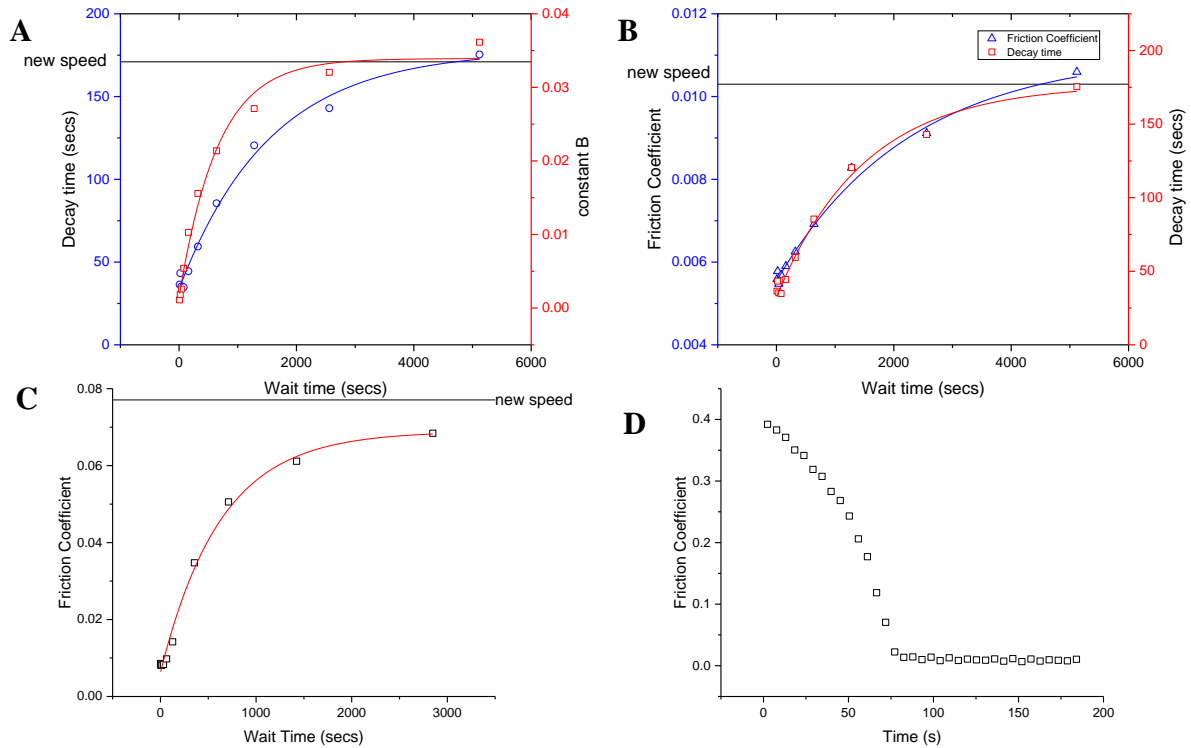


Figure 13: A) The time constant τ and constant B as defined in equation 5 v.s. wait time; Since μ is fitted with this equation, constant B is in the scale of the actual friction coefficient. The friction coefficient of PAA gel v.s. wait time for B) PAA gel on acrylic disk and C) Agarose gel on acrylic disk. Wait time is defined as the time the hydrogel is allowed to relax after being sheared at 1.27 cm/s (PAA) and 3.94cm/s (agarose) for 10 mins. The horizontal line is the average μ and τ for the friction decay when there is no prior shearing. It represents the final state of the hydrogel when $t \rightarrow \infty$. The experiment is performed 3 times. The average of these experiment is shown. All data are fitted with equation 5. D) Friction coefficient of agarose v.s. actual experimental time at $v=3.94$ cm/s. As can be seen, the decay is not exponential.

agarose seems more complicated and does not follow a pure exponential decay, as shown in Figure 13 D. The differences between PAA gels and agarose gels are expected because they have very different chemistries; for example, whereas PAA gels are permanently-crosslinked via covalent bond, agarose gels are crosslinked by intermolecular forces, which make their crosslinks more reversible.

3.5 Shear Determines the State of PAA Gel

3.5.1 Experimental Protocol

We have talked about how shearing the PAA gel above the critical shear stress will structurally alter the hydrogel, which leads to lower μ . We have also shown that the hydrogel will structurally recover back towards its original state if it is allowed to relax, but we still do not know the recovery behavior of hydrogel under shear. Here we will show how these two opposite forces compete and come to equilibrium.

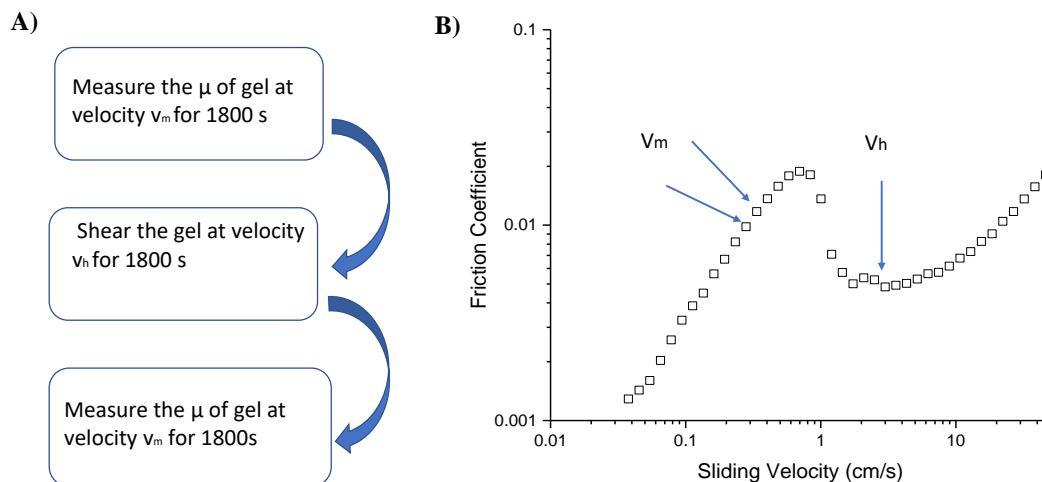


Figure 14: A) The experimental protocol in the context of B) a typical μ v.s. sliding velocity graph. The experiment is carried out with two values of v_m , which are 0.48 cm/s and 0.58cm/s. v_h is 3 cm/s.

Figure 14 shows the experimental protocol in the context of a typical μ v.s. sliding velocity graph. Two values of v_m are used. The gel is given 2 hours to fully recover between these two sets of experiment.

The point of this experiment is to see under the same shear stress how the initial state of the hydrogel will affect the μ behavior. When we measure the μ at v_m at first, the gel does not

have any prior shearing, but we shear it at v_h for 1800 s before measuring μ the second time. These two measurements, although at the same sliding velocity, have completely different initial conditions.

3.5.2 Result

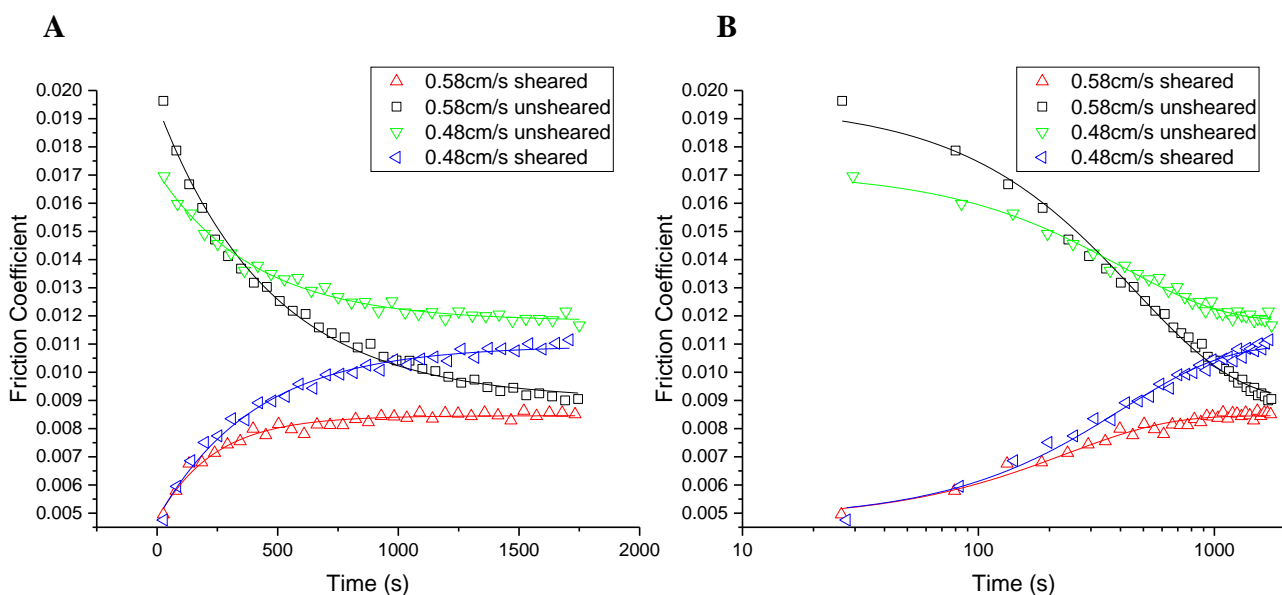


Figure 15: A) The friction coefficient of PAA gel on acrylic when it is unsheared and sheared at 3 cm/s for 30 mins before the measurement. B) The same data plotted on a log x-axis. The measurement is taken at 0.58 cm/s and 0.48 cm/s, respectively. Both 0.48 cm/s sheared and 0.58 cm/s sheared measurements start at the same value of friction coefficient. For the same sliding velocity, the μ will approach the same value as $t \rightarrow \infty$. All data are fitted with equation 5.

Figure 15 shows two μ decays and two recovery μ at 0.58 cm/s and 0.48 cm/s. The decay measurements are done in the absence of any prior shearing. The recovery measurements are performed after being sheared at 3 cm/s for 30 mins. We can see that both 0.48 cm/s sheared and 0.58 cm/s sheared measurements start at the same value of friction coefficient, which makes sense because they are both sheared at 3 cm/s for 30 mins and should be at the same state.

Figure 15 shows that although the unsheared and sheared states start at very different values of μ , if we apply the same shear stress, the μ from different initial states will approach to the same μ as $t \rightarrow \infty$. This is illustrated by the asymptotic behavior that happens both above and below the final value of μ , the μ as $t \rightarrow \infty$. In a sense, this is similar to Hooke's law, $F = k\Delta x$, in that the state of the system is determined by the external force or shear; for Hooke's law, the change in the length of the spring is determined by the external force; for our system, the final μ is determined by the sliding velocity, or equivalently shear stress.

3.6 Proposed Model

Based on our previous experimental results, we propose the following model. At the surface of the hydrogel, well-saturated polymers with free ends are expected to exist. In the absence of shear, these entangled polymers are able to move and freely explore its configuration space through thermal fluctuations, yet limited by their local proximity to the other entangled polymers. In other words, these polymers are confined in the volume determined by the local density of the entangled polymer, as shown in the dashed circle of Figure 16 A. If we apply a shear in a certain direction, this group of entangled polymer will be pulled in the direction of applied shear. As one end of this group of polymer is connected with the hydrogel, the entangled polymers will be squeezed towards the free end of the polymer, occupying a smaller volume. This smaller confinement will dramatically increase the timescale required for these entangled polymers to explore all of the configuration space, and thus it will take much longer to further disentangle.

Although this model needs further experimental verification, it is able to explain why the friction relaxation and recovery are both asymmetric. When the shear is just applied, the entangled polymers are still able to explore a big configuration space, and thus it is able to stretch in the direction of applied shear quickly, reducing the friction. However, as the entangled polymers are pushed to a smaller volume, it becomes harder for them to further

disentangle, and the rate of the friction decay also decreases. Once the shear stress applied is relieved, the entangled polymers start to retract, and there is a huge space to explore, as indicated by the red dashed circle in Figure 16 B). As the polymers retract, the size of the configuration space will decrease, lowering the rate of recovery.

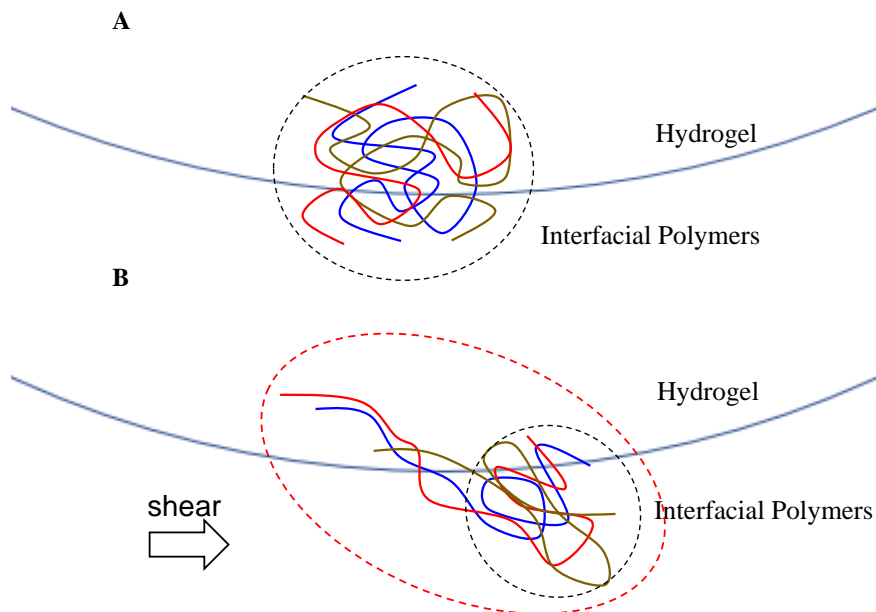


Figure 16: Potential model for friction relaxation. A) at the surface of hydrogel, polymers with free ends are expected to exist. In the absence of shear, they will be able to freely explore configuration space. B) Once a shear is applied, the group of polymer will be pulled towards the direction of the shear. The polymer entanglements will be pushed towards the end of the polymer, occupying a smaller volume.

According to our model, the relaxation and recovery of hydrogel is determined by the entropic stress of the entangled polymer

$$\sigma_{en} = \frac{k_B T}{a^3} \quad (6)$$

and applied shear

$$\sigma_{app} = \eta \frac{v}{d}, \quad (7)$$

where T is temperature in kelvin, and a is the side length of the configuration space if we model it as a cube; equation 7 is obtained from the equation 2. The entropic stress is the restoring force, driving the hydrogel back to its unsheared state.

If $\sigma_{app} < \sigma_{en}$, then the applied shear is not enough to stretch the surface polymer; the rate of recovery is much faster than any structural change in the hydrogels. If we balance σ_{app} and σ_{en} , we will get the following equation

$$v_c = \frac{k_B T d}{a^3 \eta}. \quad (8)$$

If we use the parameter $\eta = 1mPa.s$, $T = 300K$, $d \approx 50nm$, then $a \approx 30 - 50nm$ will produce the critical velocity $v_c \approx 1cm/s$ we see in our experiment. Given the size of the pore size, the length scale of a is reasonable.

4 Conclusion

Here we have examined the time-dependent behavior of PAA gel in great detail. We have shown that the time-dependent behavior is most pronounced at $0.2 < v < 20\text{cm/s}$. Inside this speed range, μ will exhibit an exponential decay behavior whose decay time and decay extent sensitively depend on the sliding velocity, or the amount of shear applied. In general, a higher sliding velocity will lead to faster decays. When the gel is fully sheared, it will recover, the rate of which is also exponentially decaying. Agarose gels tend to recover much faster than PAA gels, due to differences in chemical structures. Finally, we showed that the eventual state of the hydrogel is only controlled by the external shear stress applied, no matter what the initial state of the hydrogel is. Our current model of entangled polymers at the hydrogel surface can well capture all of our observations, although it needs future experimental verifications.

5 Future Directions

While the time-dependent behavior of PAA gels has been well understood, the decay behavior of agarose seems more complicated, and there is still much unsolved mystery. For example, the speed range for the time-dependent regime of agarose is much narrower, and it exhibits more of a logistic decay. In addition, we also need to perform additional experiments involving temperature or molecular tracking to verify our model. While McGhee et al. have done some research about how temperature change could affect the friction of Gemini hydrogels [18], they did not really look into the effect of temperature on polymer dynamics of the gels. As the rate of recovery is mainly controlled by the entropic stress of entangled polymers, we should see a faster recovery when the temperature is increased. Molecular tracking should also allow us to see how the surface polymers behave during the time-dependent regime.

References

- [1] H. Barth, S. Crafoord, S. Andréasson, and F. Ghosh. A cross-linked hyaluronic acid hydrogel as a novel vitreous substitute. *Graefes Arch. Clin. Exp. Ophthalmol.*, 254:697–703, 2016.
- [2] David J. Beebe, Jeffrey S. Moore, Joseph M. Bauer, Qing Yu, Robin H. Liu, Chelladurai Devadoss, and Byung-Ho Jo. Functional hydrogel structures for autonomous flow control inside microfluidic channels. *Nature*, 404:588–590, 2000.
- [3] Thibault Bertrand, Jorge Peixinho, Shomeek Mukhopadhyay, and Christopher W. MacMinn. Dynamics of swelling and drying in a spherical gel. *Phys. Rev. Applied*, 6:064010, Dec 2016.
- [4] Nicholas L. Cuccia, Suraj Pothineni, Brady Wu, Joshua Méndez-Harper, and Justin C. Burton. Pore-size dependence and slow relaxation of hydrogel friction on smooth surfaces, 2020.
- [5] Liang Dong, Abhishek K. Agarwal, David J. Beebe, and Hongrui Jiang. Adaptive liquid microlenses activated by stimuli-responsive hydrogels. *Nature*, 442:551–554, 2006.
- [6] Jian Ping Gong. Friction and lubrication of hydrogels—its richness and complexity. *Soft Matter*, 2:544–552, 2006.
- [7] Jianping Gong, Megumi Higa, Yoshiyuki Iwasaki, Yoshinori Katsuyama, and Yoshihito Osada. Friction of gels. *The Journal of Physical Chemistry B*, 101:5487–5489, 1998.
- [8] Jianping Gong and Yoshihito Osada. Gel friction: A model based on surface repulsion and adsorption. *J. Chem. Phys.*, 109:8062–8068, 1998.
- [9] G. W. Greene, X. Banquy, D. W. Lee, D. D. Lowrey, J. Yu, and J. N. Israelachvili. Adaptive mechanically controlled lubrication mechanism found in articular joints. *Proc. Natl. Acad. Sci. U.S.A.*, 108:5255–5259, 2011.

- [10] Marcos R. Guilherme, Fauze A. Aouada, André R. Fajardo, Alessandro F. Martins, Alexandre T. Paulino, Magali F.T. Davi, Adley F. Rubira, and Edvani C. Muniz. Superabsorbent hydrogels based on polysaccharides for application in agriculture as soil conditioner and nutrient carrier: A review. *Eur. Polym. J.*, 72:365–385, 2015.
- [11] Mehrdad Hamidi, Amir Azadi, and Pedram Rafiei. Hydrogel nanoparticles in drug delivery. *Adv. Drug Delivery Rev.*, 60:1638–1649, 2008.
- [12] J. Kim and A.C Dunn. Thixotropic mechanics in soft hydrated sliding interfaces. *Tribol. Lett.*, 66, 2018.
- [13] J. Kisiday, M. Jin, B. Kurz, H. Hung, C. Semino, S. Zhang, and A. J. Grodzinsky. Self-assembling peptide hydrogel fosters chondrocyte extracellular matrix production and cell division: Implications for cartilage tissue repair. *Proc. Natl. Acad. Sci. U.S.A.*, 99:9996–10001, 2002.
- [14] C. Larson, B. Peele, S. Li, S. Robinson, M. Totaro, L. Beccai, B. Mazzolai, and R. Shepherd. Highly stretchable electroluminescent skin for optical signaling and tactile sensing. *Science*, 351:1071–1074, 2016.
- [15] Kuen Yong Lee and David J. Mooney. Hydrogels for tissue engineering. *Chem. Rev.*, 101:1869–1880, 2001.
- [16] Oliver Lieleg and Katharina Ribbeck. Biological hydrogels as selective diffusion barriers. *Trends Cell Biol.*, 21:543–551, 2011.
- [17] Liran Ma, Anastasia Gaisinskaya-Kipnis, Nir Kampf, and Jacob Klein. Origins of hydration lubrication. *Nat. Commun.*, 6:6060, 2015.
- [18] E. O. McGhee, J. M. Urue na, A. A. Pitenis, and W. G. Sawyer. Temperature-dependent friction of gemini hydrogels. *Tribol. Lett.*, 67:67–117, 2019.

- [19] A. C. Moore, J. F. DeLucca, D. M. Elliott, and D. L. Burris. Quantifying cartilage contact modulus, tension modulus, and permeability with hertzian biphasic creep. *J. Tribol.*, 138:041405, 2016.
- [20] A.C. Moore and D.L. Burris. An analytical model to predict interstitial lubrication of cartilage in migrating contact areas. *J. Biomech.*, 47:148–153, 2014.
- [21] A.C. Moore and D.L. Burris. Tribological and material properties for cartilage of and throughout the bovine stifle: support for the altered joint kinematics hypothesis of osteoarthritis. *Osteoarthr. Cartilage*, 23:161–169, 2015.
- [22] A.C. Moore and D.L. Burris. Tribological rehydration of cartilage and its potential role in preserving joint health. *Osteoarthr. Cartilage*, 25:99–107, 2017.
- [23] Anupam Pandey, Stefan Karpitschka, Cornelis H. Venner, and Jacco H. Snoeijer. Lubrication of soft viscoelastic solids. *J. Fluid Mech.*, 799:433–447, 2016.
- [24] Uri Raviv and Jacob Klein. Fluidity of bound hydration layers. *Science*, 297:1540–1543, 2002.
- [25] E. R. Reale and A. C. Dunn. Poroelasticity-driven lubrication in hydrogel interfaces. *Soft Matter*, 13:428, 2017.
- [26] A. C. Rennie, P. L. Dickrell, and W. G. Sawyer. Friction coefficient of soft contact lenses: measurements and modeling. *Tribol. Lett.*, 18:499–504, 2005.
- [27] W. M. Rhee, F. A. Delustro, and R. A. Berg. Method for treating or inhibiting the formation of adhesions following surgery or injury, 2012.
- [28] Baudouin Saintyves, Theo Jules, Thomas Salez, and L. Mahadevan. Self-sustained lift and low friction via soft lubrication. *Proc. Natl. Acad. Sci. U.S.A.*, 113:5847–5849, 2016.

- [29] T. Shoaib, J. Heintz, J. A. Lopez-Berganza, R. Muro-Barrios, S. A. Egner, and R. M. Espinosa-Marzal. Stick-slip friction reveals hydrogel lubrication mechanisms. *Langmuir*, 34:756–765, 2017.
- [30] A. Sidorenko, T. Krupenkin, A. Taylor, P. Fratzl, and J. Aizenberg. Reversible switching of hydrogel-actuated nanostructures into complex micropatterns. *Science*, 315:487–490, 2007.
- [31] J. M. Skotheim and L. Mahadevan. Soft lubrication. *Phys. Rev. Lett.*, 92:245509, 2004.
- [32] J. M. Skotheim and L. Mahadevan. Soft lubrication: The elastohydrodynamics of nonconforming and conforming contacts. *Phys. Fluids*, 17:092101, 2005.
- [33] J. H. Snoeijer, J. Eggers, and C. H. Venner. Similarity theory of lubricated hertzian contacts. *Phys. Fluids*, 25:101705, 2013.
- [34] Jeong-Yun Sun, Xuanhe Zhao, Widusha R. K. Illeperuma, Ovijit Chaudhuri, Kyu Hwan Oh, David J. Mooney, Joost J. Vlassak, and Zhigang Suo. Highly stretchable and tough hydrogels. *Nature*, 489:133–136, 2012.
- [35] Javier Urzay, Stefan G. Llewellyn Smith, and Beverley J. Glover. The elastohydrodynamic force on a sphere near a soft wall. *Phys. Fluids*, 19:103106, 2007.
- [36] Tetsurou Yamamoto, Takayuki Kurokawa, Jamil Ahmed, Gen Kamita, Shintaro Yashima, Yuichiro Furukawa, Yuko Ota, Hidemitsu Furukawa, and Jian Ping Gong. In situ observation of a hydrogel–glass interface during sliding friction. *Soft Matter*, 10:5589–5596, 2014.